7244 *Inorg. Chem.* **2009**, *48*, 7244–7250
DOI: 10.1021/ic9006857

Inorganic Chemistry
Article

Long-Distance Magnetic Interaction of Exchange-Coupled Copper Dimers with Nitronyl Nitroxide and *tert*-Butyl Nitroxide Radicals

Martin Jung,[†] Ajay Sharma,[‡] Dariush Hinderberger,[‡] Sebastian Braun,[§] Ulrich Schatzschneider,[§] and Eva Rentschler*,[†]

[†]*Institut für Anorganische Chemie und Analytische Chemie, Johannes-Gutenberg-Universität Mainz, Duesbergweg 10-14, D-55128 Mainz, Germany,* [‡]*Max-Planck-Institut für Polymerforschung, Ackermannweg 10, D-55128 Mainz, Germany, and* [§]*Lehrstuhl für Anorganische Chemie I - Bioanorganische Chemie, Ruhr-Universität Bochum NC 3/74, Universitätsstrasse 150, D-44801 Bochum, Germany*

Received April 8, 2009

To study long-distance magnetic interactions between exchange-coupled metal centers and coordinated radical moieties, two new homodimetallic Cu(II) complexes held together by the chelating ligand L^{nPr} = *N*,*N*,*N*′,*N*′-tetrakis-(*N*-propyl-2-benzimidazolyl)-2-hydroxy-1,3-diaminopropane and additionally bridged by either a nitronyl nitroxide (NIT) or a *tert*-butyl nitroxide (NOA) radical-substituted benzoate have been prepared. The complexes have been investigated by X-ray crystallography, magnetic susceptibility measurements, electron paramagnetic resonance (EPR) spectroscopy, and density functional theory (DFT) calculations. For comparison additionally the related copper dimer with the bridging diamagnetic nitrobenzoate ligand was investigated. Magnetic susceptibility measurements on powdered samples reveal a ferromagnetic interaction between the copper ions of $J_{Cu-Cu} = +28\ cm^{-1}$ for all three compounds. The NIT-bridged dimer additionally shows a metal-radical interaction of $J'_{Cu\text{-}NIT} = -2.3\ cm^{-1}$ while in the case of the NOA radical, the coupling becomes weakly ferromagnetic with $J'_{Cu\text{-}NOA} = +1.1\ cm^{-1}$. This contrasting behavior is explained by the different effective spin-polarization mechanism present. The magnetic data that show for the first time a significant long distance exchange interaction between a peripheral radical unit and a metal dimer were confirmed by EPR spectroscopy and DFT calculations.

Introduction

For the investigation of molecule-based magnetic systems metal-radical compounds play an important role. Research so far has focused in particular on the nitronyl nitroxide (NIT) family of radicals since they are stable and easy to functionalize. In the so-called "metal-radical approach" strong exchange interactions between stable radicals and coordinated open-shell transition metals ions were established.[1] When applying this approach to NIT radicals as bis-monodentate ligands toward metal ions, usually low-dimensional systems are obtained. Since NIT radicals are poorly donating ligands, the use of strongly electron-withdrawing coligands at the metal, like hexafluoroacetylacetonate (hfac), is required. However, the steric demand of the coligands restricts the dimensionality of the resulting metal-radical compounds. Thus a large number of linear chain compounds were prepared by this strategy, some of them recently received significant attention because of their behavior as single chain magnets.[2,3] Low-dimensional larger ring systems with spin ground states as high as $S = 12$ also have been obtained,[4] and finally two-dimensional (2D) magnetically ordered systems with a critical temperature of $T_c = 52$ K were reported, using bis-bidentate imidazolato- and benzimidazolato-NIT radicals.[5,6] Recent work has concentrated on NIT radicals that carry electron-donating substituents like 2-pyridine,[7−9] 2,2′-bipyridine,[10,11]

*To whom correspondence should be addressed. E-mail: rentschler@uni-mainz.de. Fax: +49 6131 39 23922.

(1) Caneschi, A.; Gatteschi, D.; Sessoli, R.; Rey, P. *Acc. Chem. Res.* **1989**, *22*, 392.
(2) Caneschi, A.; Gatteschi, D.; Lalioti, N.; Sangregorio, C.; Sessoli, R.; Venturi, G.; Vindigni, A.; Rettori, A.; Pini, M. G.; Novak, M. A. *Angew. Chem., Int. Ed.* **2001**, *40*, 1760.
(3) Bogani, L.; Vindigni, A.; Sessoli, R.; Gatteschi, D. *J. Mater. Chem.* **2008**, *18*, 4750.
(4) Caneschi, A.; Gatteschi, D.; Laugier, J.; Rey, P.; Sessoli, R.; Zanchini, C. *J. Am. Chem. Soc.* **1988**, *110*, 2795.
(5) Luneau, D.; Rey, P. *Coord. Chem. Rev.* **2005**, *249*, 2591.
(6) Luneau, D.; Borta, A.; Chumakov, Y.; Jacquot, J.-F.; Jeanneau, E.; Lescop, C.; Rey, P. *Inorg. Chim. Acta* **2008**, *361*, 3669.
(7) Rajadurai, C.; Ostrovsky, S.; Falk, K.; Enkelmann, V.; Haase, W.; Baumgarten, M. *Inorg. Chim. Acta* **2004**, *357*, 581.
(8) Yamamoto, Y.; Yoshida, T.; Suzuki, T.; Kaizaki, S. *Inorg. Chim. Acta* **2001**, *325*, 187.
(9) Liu, Z. L.; Lu, Z. L.; Zhang, D. Q.; Jiang, Z. H.; Li, L. C.; Liu, C. M.; Zhu, D. B. *Inorg. Chem.* **2004**, *43*, 6620.
(10) Luneau, D.; Romero, F. M.; Ziessel, R. *Inorg. Chem.* **1998**, *37*, 5078.
(11) Romero, F. M.; Luneau, D.; Ziessel, R. *Chem. Commun.* **1998**, 551.
(12) Fegy, K.; Luneau, D.; Belorizky, E.; Novac, M.; Tholence, J. L.; Paulsen, C.; Ohm, T.; Rey, P. *Inorg. Chem.* **1998**, *37*, 4524.
(13) Fegy, K.; Luneau, D.; Ohm, T.; Paulsen, C.; Rey, P. *Angew. Chem., Int. Ed. Engl.* **1998**, *37*, 1270.
(14) Fegy, K.; Sanz, N.; Luneau, D.; Belorizky, E.; Rey, P. *Inorg. Chem.* **1998**, *37*, 4518.

Published on Web 07/02/2009

imidazole,[12,13] benzimidazole,[14−16] or 1,2,4-triazole,[17−22] to avoid the necessity of coligands by taking advantage of the chelate effect of a nitrogen donor in *ortho*-position to the NIT moiety. However, this usually leads to small, discrete molecules. Hence additional exchange interaction pathways have to be introduced if one wants to arrive at either high spin-ground state metal-radical clusters at 2D and three-dimensional (3D) extended systems with high ordering temperatures. In previous work, we were able to show that weak long-distance magnetic interactions between the spin-carrying NIT moiety and coordinated paramagnetic metal ions arise even if the ligands are only bound via an additional functional group in the periphery of a phenyl ring attached to the NIT. In the case of *para*-phenolate as the functional group coordinating a nickel ion, long distance intramolecular spin exchange interactions over 9 Å could be detected.[23] However, in terms of versatility in coordination chemistry, the carboxylate group is a much more appealing functionality as anchoring or bridging group to or between metal ions, respectively. In particular, we used radical-functionalized benzoates to synthesize molecular clusters that typically employ diamagnetic acetates or pivalates. In recent work, we found that for NIT-substituted benzoates, a spin-exchange is not observable for molecules in which homovalent metal dimers are antiferromagnetically coupled,[24,25] because of the diamagnetic ground state of the metal unit. Also, in the case of an antiferromagnetically coupled heterovalent Mn(III,IV) dimer with a $S = 1/2$ ground state, only a very weak antiferromagnetic metal-radical interaction of $J_{\text{NIT-Mn}} = (1 \pm 1)\ \text{cm}^{-1}$ was observed.[26,27] To obtain high spin ground states the use of ferromagnetically coupled metal dimers is more promising. Here, we report on the structural and magnetic properties of such a dimetal unit bridged by either a NIT- or a *tert*-butyl nitroxide-substituted benzoate.

Results and Discussion

Dinuclear copper(II) complexes chelated by deprotonated ligand *N*,*N*,*N*′,*N*′-tetrakis(*n*-propyl-2-benzimidazolyl)-2-hydroxy-1,3-diaminopropane (L^{nPr}) and bridged by either $O_2N-C_6H_4-COO^-$, $NIT-C_6H_4-COO^-$, or $NOA-C_6H_4-COO^-$ (Chart 1) were prepared by mixing the constituents in methanol followed by recrystallization of the precipitated crude product from acetonitrile/diethylether.

Chart 1. Structure of Ligands L^{nPr}, $NIT-C_6H_4-COO^-$ and $NOA-C_6H_4-COO^-$ Used in This Work

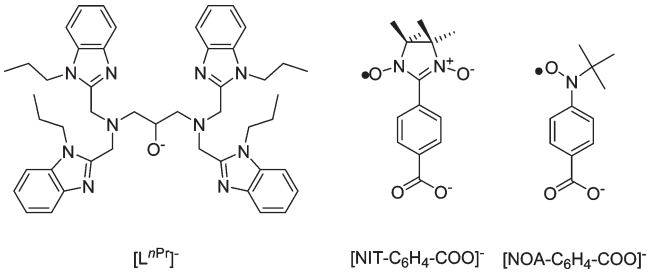

Table 1. Summary of the X-ray Crystal Structure Data Collection and Refinement for **1**, **2**, and **3**

	1	**2**	**3**
Fw	1294.9	3002.9	1503.7
space group	triclinic $P\bar{1}$	monoclinic $C2/n$	triclinic $P\bar{1}$
a, Å	13.9847(3)	27.9306(32)	13.9956(30)
b, Å	15.8383(3)	17.8984(21)	15.9833(33)
c, Å	15.8321(3)	33.8368(39)	16.9550(35)
α, deg	72.9618(10)	90.0	74.888(13)
β, deg	65.3527(10)	121.437(4)	85.890(12)
γ, deg	84.5170(10)	90.0	68.186(12)
V, Å^3	3045.91(11)	14432.51(415)	3398.07(221)
Z	2	4	2
T, K	171(2)	171(2)	171(2)
ρ calcd, g cm^{-1}	1.41	1.38	1.42
μ(Mo-*K*α), cm^{-1}	0.780	0.735	0.762
refl. collected	77349	110788	57886
unique refl. [$I > 2\sigma(I)$]	14369/6356	17308/6479	14210/2503
no. parameters	833	904	837
Θ_{max}, deg	27.81	28.1	27.6
R^a [$I > 2\sigma(I)$]	0.073	0.058	0.116
wR^a [$I > 2\sigma(I)$]	0.209	0.107	0.283

[a] $w = 1/[\sigma^2(F_o^2) + (xP)^2]$ where $P = (F_o^2 + 2F_c^2)/3$ and $x = 0.1335$ for **1**, $x = 0.0389$ for **2**, and $x = 0.18210$ for **3**.

All three complexes gave satisfactory elemental analysis and could be characterized by X-ray crystallography. Relevant information on the data collection and refinement are summarized in Table 1.

Crystal and Molecular Structure of $[Cu_2(L^{nPr})(O_2N-C_6H_4-COO)](BF_4)_2 \cdot CH_3CN$, 1. In this complex, both copper(II) centers have a trigonal-bipyramidal coordination environment with τ values of $\tau = 0.92$ for Cu(1) and $\tau = 0.84$ for Cu(2), respectively.[28] The Cu(1)−O(1)−Cu(2) angle is 128.60(17)°. The axial positions at the copper centers Cu(1) and Cu(2) are occupied by the carboxylate oxygen atoms O(2) and O(3), as well as the amine nitrogens N(1) and N(4), respectively, while two benzimidazole nitrogen donor atoms and the bridging oxygen O(1) are in the trigonal plane (Figure 1). The phenyl ring of the benzoate ligand is tilted relative to the carboxylate group by an angle of 3.8°, which is comparable to the other compounds. In the diamagnetic ligand framework, no short intermolecular contacts to the metal centers are present in **1**, although the nitrobenzoates of two neighboring molecules show a $\pi-\pi$-stacking with a distance of 3.5 Å.

(15) Lescop, C.; Belorizky, E.; Luneau, D.; Rey, P. *Inorg. Chem.* **2002**, *41*, 3375.
(16) Lescop, C.; Luneau, D.; Bussiere, G.; Triest, H.; Reber, C. *Inorg. Chem.* **2000**, *39*, 3740.
(17) Pei, Y.; Kahn, O.; Aebersold, M. A.; Ouahab, L.; Leberre, F.; Pardi, L.; Tholence, J. L. *Adv. Mater.* **1994**, *6*, 681.
(18) Lang, A.; Pei, Y.; Ouahab, L.; Kahn, O. *Adv. Mater.* **1996**, *8*, 60.
(19) Pei, Y.; Lang, A.; Bergerat, P.; Kahn, O.; Fettouhi, M.; Ouahab, L. *Inorg. Chem.* **1996**, *35*, 193.
(20) Daro, N.; Guionneau, P.; Golhen, S.; Chasseau, D.; Ouahab, L.; Sutter, J. P. *Inorg. Chim. Acta* **2001**, *326*, 47.
(21) Sutter, J. P.; Kahn, M. L.; Golhen, S.; Ouahab, L.; Kahn, O. *Chem. Eur. J.* **1998**, *4*, 571.
(22) Kahn, M. L.; Sutter, J. P.; Golhen, S.; Guionneau, P.; Ouahab, L.; Kahn, O.; Chasseau, D. *J. Am. Chem. Soc.* **2000**, *122*, 3413.
(23) Schatzschneider, U.; Weyhermuller, T.; Rentschler, E. *Eur. J. Inorg. Chem.* **2001**, 2569.
(24) Schatzschneider, U.; Weyhermüller, T.; Rentschler, E. *Inorg. Chim. Acta* **2002**, *337*, 122.
(25) Jung, M.; Sharma, A.; Hinderberger, D.; Braun, S.; Schatzschneider, U.; Rentschler, E. *Eur. J. Inorg. Chem.* **2009**, 1495.
(26) Marlin, D. S.; Bill, E.; Weyhermüller, T.; Rentschler, E.; Wieghardt, K. *Angew. Chem., Int. Ed.* **2002**, *41*, 4775.
(27) Marlin, D. S.; Bill, E.; Weyhermüller, T.; Bothe, E.; Wieghardt, K. *J. Am. Chem. Soc.* **2005**, *127*, 6095.
(28) Addison, A. W.; Rao, T. N.; Reedijk, J.; Vanrijn, J.; Verschoor, G. C. *J. Chem. Soc., Dalton Trans.* **1984**, 1349.

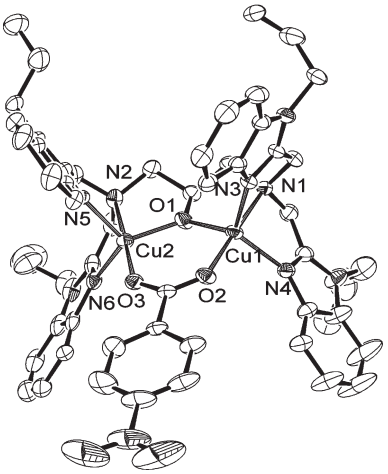

Figure 1. Molecular structure of **1**. Counterions, hydrogen atoms, and solvate molecules are not shown. Ellipsoids are drawn at the 25% probability level.

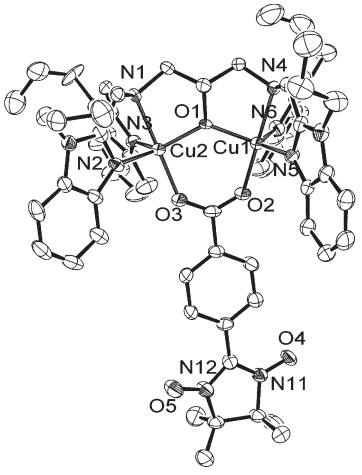

Figure 2. Molecular structure of **2**. Counterions, hydrogen atoms, and solvate acetonitrile molecules are not shown. Ellipsoids are drawn at the 50% probability level.

Crystal and Molecular Structure of $[Cu_2(L^{nPr})(NIT-C_6H_4-COO)](ClO_4)_2\cdot 3CH_3CN$, 2. In the NIT compound **2**, the ligand arrangement around the copper centers is essentially identical to **1**. Both coordination environments are trigonal-bipyramidal with $\tau = 0.91$ for Cu(1) and $\tau = 0.82$ for Cu(2). The Cu(1)−O(1)−Cu(2) angle is 129.34(1)°, similar to the nitrobenzoate complex **1**. The phenyl ring of the NIT-benzoate is tilted relative to the carboxylate group by an angle of 6.1° while the tilt angle between the phenyl ring and the mean plane of the NIT group is 11.5° (Figure 2). This is rather small compared to angles of around 35° to 45° reported for other NIT ligands.[24,26,29] In compound **2**, short intermolecular contacts between spin-bearing moieties are absent. The closest distances, < 4 Å, of the NO groups from the NIT involve only the diamagnetic ligand framework. Thus, the complex can be considered as magnetically isolated in the solid state.

Crystal and Molecular Structure of $[Cu_2(L^{nPr})(NOA-C_6H_4-COO)](PF_6)_2\cdot 0.5MeOH\cdot 2H_2O$, 3. In the *tert*-butyl nitroxide complex, the two copper(II) centers also have a

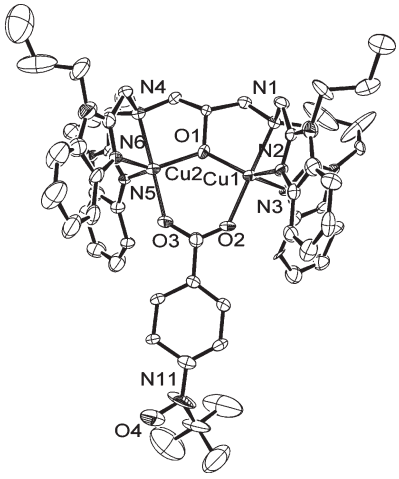

Figure 3. Molecular structure of **3**. Counterions, hydrogen atoms, and solvate water as well as ether molecules are not shown. Ellipsoids are drawn at the 25% probability level.

trigonal-bipyramidal coordination environment with $\tau = 0.94$ for Cu(1) and $\tau = 0.87$ for Cu(2). The Cu(1)−O(1)−Cu(2) angle is 131.5(5)° and thus does not differ significantly from that observed in **1** and **2**. The phenyl ring of the NOA-benzoate is tilted relative to the carboxylate group by an angle of 10.6° while the tilt angle between the phenyl ring and the N−O vector of the NOA group is 55.7° (Figure 3). This value is significantly larger than the one observed for the free NOA-benzoate of 18.3°[30] and is caused by packing effects. Short intermolecular contacts between spin-bearing moieties are absent in **3**. One of the benzimidazole rings has a short intermolecular distance of 3.8 Å to a neighboring benzimidazole group. The shortest distances, < 4 Å, to the NO group involve only the diamagnetic ligand framework. Thus, intermolecular exchange interactions should be absent in this complex.

Magnetic Properties of Complexes 1 to 3. To unambiguously determine the exchange coupling between the two metal ions, the temperature dependence of the molar magnetic susceptibility of nitrobenzoate-bridged complex **1** was measured in the temperature range of 2 to 300 K. The $\chi_m T$ value steadily increases upon lowering the temperature from 0.9 $cm^3\cdot K\cdot mol^{-1}$ at 300 K to 1.15 $cm^3\cdot K\cdot mol^{-1}$ at 8 K before decreasing again at very low temperatures (Figure 4), indicative of an intramolecular ferromagnetic exchange interaction. The data were modeled using the appropriate Heisenberg−Dirac−Van-Vleck (HDVV) spin Hamiltonian[31,32] for isotropic exchange [eq 1].[33]

A good fit was obtained for the dicopper complex **1** with $g_{Cu} = 2.15$, which is a reasonable value for copper(II) ions with considerable angular momentum. The exchange parameter was determined as $J_{Cu-Cu} = +28.0\ cm^{-1}$.

$$\check{H} = -2\cdot J\cdot \hat{S}_{M1}\cdot \hat{S}_{M2} \qquad (1)$$

(29) Schiodt, N. C.; deBiani, F. F.; Caneschi, A.; Gatteschi, D. *Inorg. Chim. Acta* **1996**, *248*, 139.

(30) Maspoch, D.; Catala, L.; Gerbier, P.; Ruiz-Molina, D.; Vidal-Gancedo, J.; Wurst, K.; Rovira, C.; Veciana, J. *Chem.—Eur. J.* **2002**, *8*, 3635.

(31) J. H. Van Vleck *The theory of electric and magnetic susceptibilities*; Oxford Press: London, 1932.

(32) Kahn, O. *Molecular magnetism*; VCH: New York, 1993.

(33) Simulation of the experimental magnetic data with a full-matrix diagonalisation approach was performed with the julX program developed by E. Bill / Max-Planck-Institute for Bioinorganic Chemistry.

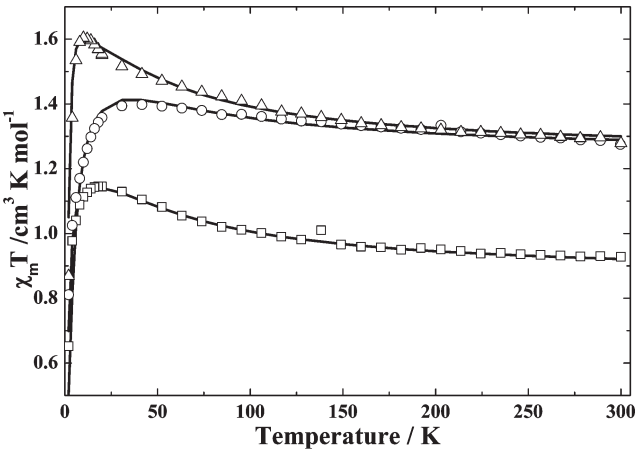

Figure 4. Temperature dependence of the molar magnetic susceptibility as function of $\chi_m T$ for **1** (□), **2** (○), and **3** (△); solid lines: simulation of the experimental data, see text for parameters.

The plots of the molar magnetic susceptibility as a function of $\chi_m T$ versus temperature for the metal-radical complexes **2** and **3** are also shown in Figure 4. At 300 K, both compounds show a room temperature $\chi_m T$ value of 1.3 $cm^3 \cdot K \cdot mol^{-1}$, which is 0.4 $cm^3 \cdot K \cdot mol^{-1}$ higher than for the diamagnetic nitrobenzoate compound and thus confirms the additional magnetic contribution of the NIT and NOA radicals, respectively. For compound **2**, the increase of $\chi_m T$ upon lowering the temperature is clearly less prominent than observed for **1**. It steadily increases to a value of 1.4 $cm^3 \cdot K \cdot mol^{-1}$ at 30 K and then shows a significant decrease at lower temperatures. This is indicative of the existence of an additional effective antiferromagnetic exchange interaction between the triplet state of the copper dimer and the NIT radical. For compound **3**, the $\chi_m T$ value steadily increases upon lowering the temperature to a maximum value of 1.60 $cm^3 \cdot K \cdot mol^{-1}$ at 5 K before decreasing at very low temperatures. The more pronounced increase in $\chi_m T$ for **3** compared to **1** indicates an additional weak ferromagnetic interaction between the ferromagnetically coupled copper ions and the NOA radical. The $\chi_m T$ versus T curves for complexes **2** and **3** were simulated using the same parameter set as for compound **1**, with $g_{Cu} = 2.15$ and $J_{Cu-Cu} = +28.0$ cm^{-1}. For NIT complex **2**, the additional exchange coupling for the metal-radical interaction was included with $J'_{Cu\text{-}NIT} = -2.3$ cm^{-1}. For compound **3**, a metal-radical interaction of $J'_{Cu\text{-}NOA} = +1.2$ cm^{-1} was determined using the Hamiltonian in eq 2.

$$\check{H} = -2 \cdot J \cdot (\hat{S}_{M1} \cdot \hat{S}_{M2}) - 2 \cdot J' \cdot (\hat{S}_{M1} \cdot \hat{S}_{rad} + \hat{S}_{M2} \cdot \hat{S}_{rad}) \quad (2)$$

The ferromagnetic coupling between the copper(II) centers is comparable to similar alkoxo-carboxylato bridged dicopper complexes[34,35] and can be attributed to the counter-complementary effect, which is known for bis-bridged copper dimers.[36−39] However, the ferromagnetic coupling can also be rationalized by inspection of the relative orientations of the d_{z^2} orbitals of the copper(II) ions. In trigonal-bipyramidal coordination, these are the singly occupied molecular orbitals, and their orientation leads to a vanishing overlap integral along the μ-alkoxo bridge as well as the carboxylate group, thus leading to a ferromagnetic exchange interaction. The same parameter set for **1**, **2**, and **3** is justified by the very similar ligand environment and binding mode in all three compounds. The different sign of the metal-radical interaction in **2** and **3** is explained by spin-polarization effects. In the case of **2**, this leads to a spin projection with antiparallel spin alignment, thus confirming the antiferromagnetic exchange interaction between the dicopper unit and the radical, while upon shortening the exchange path, a parallel alignment is expected for **3**. Thus, for the first time, a significant long-distance magnetic interaction between two metal centers and a peripheral radical unit could be proven by magnetic measurements. Moreover, compounds **2** and **3** nicely illustrate the directed control on the sign of the exchange interaction by application of the easy but charming approach of spin polarization.

EPR Spectroscopy. To confirm the different magnetic behavior of compounds **1**, **2**, and **3**, additional electron paramagnetic resonance (EPR) spectroscopic measurements were carried out. The X-band EPR spectrum of a frozen solution of **1** at 10 K shows a broadened hyperfine pattern of copper. The simulation of the spectrum gives a rhombic g-tensor with $g_x = 2.18$, $g_y = 2.11$, and $g_z = 2.05$. The rhombic hyperfine tensor has the components $A_x = 12.0$, $A_y = 4.0$, and $A_z = 0.5$ mT. The hyperfine parameters are approximately half of the values which are found for monomeric copper species[40] and confirm the existence of the bimetallic unit.

The EPR spectra of **2** in frozen solution show a broadened signal at $g_{average} = 2.08$ (see Figure 6) without any Cu (II) hyperfine features (compare Figure 5 and Figure 6). The $g_{average}$ of **2** (2.08) is much closer to the free electron g-value (2.0023) when compared with $g_{average}$ of **1** (2.11). In addition, there is no signature of Cu (II) hyperfine lines observable in the spectra. The hyperfine lines may be weak and broadened and thus may be merged within the broad central line which is due to the delocalization of spin density from Cu dimer to the NIT radical. The EPR spectra could be simulated assuming an $S = 1/2$ spin ground state which arises from the weak antiferromagnetic interaction of the NIT radical with the ferromagnetically coupled copper dimer as also observed from SQUID measurements. The absence of any clear Cu (II) hyperfine pattern also indicates the existence of the Kramer's doublet ($S = 1/2$, $m_s = \pm 1/2$) arising from the coupling of the radical with the copper triplet state. At lower fields unresolved transitions of unknown origin are observed, which, however, were too broad to be considered in the simulation of the spectra.

The spectra of **3** show a weak signal at $g \sim 2$ and a strong signal at $g \sim 4$, characteristic for an $S = 3/2$ system in the

(34) McKee, V.; Zvagulis, M.; Dagdigian, J. V.; Patch, M. G.; Reed, C. A. *J. Am. Chem. Soc.* **1984**, *106*, 4765.
(35) Nishida, Y.; Yatani, A.; Nakao, Y.; Taka, J.; Kashino, S.; Mori, W.; Suzuki, S. *Chem. Lett.* **1999**, 135.
(36) Nishida, Y.; Takeuchi, M.; Takahashi, K.; Kida, S. *Chem. Lett.* **1985**, 631.
(37) Hay, P. J.; Thibeault, J. C.; Hoffmann, R. *J. Am. Chem. Soc.* **1975**, *97*, 4884.
(38) Nishida, Y.; Kida, S. *J. Chem. Soc., DaltonTrans.* **1986**, 2633.
(39) McKee, V.; Zvagulis, M.; Reed, C. A. *Inorg. Chem.* **1985**, *24*, 2914.
(40) Bencini, A.; Gatteschi, D. *Electron paramagnetic resonance of exchange coupled systems*; Springer-Verlag: Berlin, 1990.

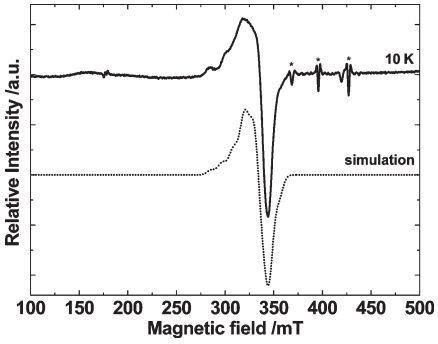

Figure 5. CW EPR spectrum of a frozen solution of **1** (20 mM in acetonitrile at 10 K). The dotted line represents the simulation of the spectrum, see the text for parameters. Peaks caused by instrumental errors are marked by asterisks.

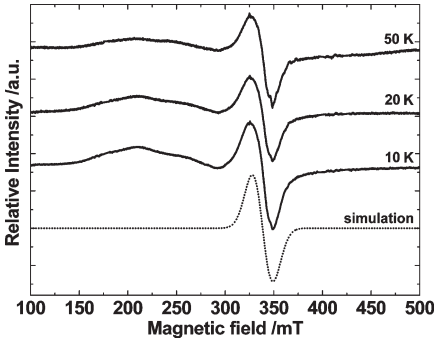

Figure 6. Temperature dependence of the CW EPR signal of a frozen solution of **2** (20 mM in acetonitrile at 10 K, 20 K, and 50 K). The dotted line represents the simulation of the spectrum, see text for parameters.

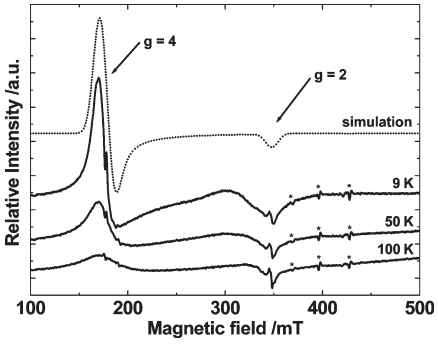

Figure 7. Temperature dependence of the CW EPR signal of a frozen solution of **3** (20 mM in acetonitrile at 9 K, 50 K, and 100 K). The dotted line represents the simulation of the spectrum, see text for parameters. Peaks caused by instrumental errors are marked by asterisks.

presence of a zero-field-splitting (ZFS) larger than the EPR microwave energy ($|D| \gg 0.3$ cm^{-1}, see Figure 7).[41,42] EPR simulations using the standard spin Hamiltonian for an $S = 3/2$ system successfully reproduce the experimental spectra. The g values used for the simulation are $g_{x,y} = 2.05$, $g_z = 2$. The ZFS splits the $S = 3/2$ quartet into two Kramer's doublets ($m_s = \pm 1/2$ and $m_s = \pm 3/2$). For the case when the ZFS is much larger than the EPR microwave energy ($|D| \gg 0.3$ cm^{-1}), transitions only within the respective $\pm 1/2$ and $\pm 3/2$ Kramer's doublets are possible, and the intermixing of these states ($\pm 1/2$ and $\pm$ 3/2) can be ignored. In a Kramer's doublet, the g-anisotropy can become very large and in our case leads to a quasi-axial g-tensor with $g_\perp \sim 4$ (which is equal to twice the "true" $g_{x,y}$ ($g = 2g_{x,y}$) of the molecule) and the weak signal at $g_{||} \sim 2$, which both stem from transitions between the $\pm 1/2$ levels of the $S = 3/2$ spin system with the outer magnetic field perpendicular ($g_\perp$) and parallel ($g_{||}$) to the unique molecular axis (z), respectively.[40,41] The intensity of the transition at $g \sim 4$ decreases drastically with increase of temperature (from 9 to 50 K), which indicates that the weak coupling between the Cu dimer and the NOA radical is ferromagnetic. The ratio E/D can be determined as ~ 0.025 from a limiting value of $|D| \geq 0.8$ cm^{-1}. This ZFS is too small to be observed in the magnetic susceptibility measurements. Comparison of the EPR spectra for all three compounds clearly shows the difference in the lowest-lying magnetic states of $S = 1$, $S = 1/2$, and $S = 3/2$ for **1**, **2**, and **3**, respectively.

Density Functional Calculations. The interpretation of the experimental results is supported by density functional theory (DFT) calculations of the energies of the different spin states of compounds **2** and **3** at the UB3LYP level. Using the coordinates from the X-ray structure determinations, without any geometric relaxation and very strict convergence, semiquantitative results can be obtained. Starting from the high-spin state data all relevant lower spin states could be converged. For both **2** and **3**, three $S = 1/2$ states were characterized, one with the spin of the organic radical antiparallel to the ferromagnetically coupled dimetal unit, as well as two states in which the metals are antiferromagnetically coupled and the radical spin is parallel to one or the other metal center. These latter two states were found to be nearly degenerate and thus these systems were treated as symmetrical triangular. Using the Hamiltonian eq 2 with

$$\hat{S} = \hat{S}_{M1} + \hat{S}_{M2}$$

and

$$\hat{S}' = \hat{S} + \hat{S}_{\mathrm{rad}}$$

one then obtains for the energies of the spin states in zero field.

$$E(S', S) = -J'S'(S'+1) - (J - J')S(S+1) \qquad (3)$$

In Table 2, the calculated exchange coupling parameters J and J' are compared to the experimental ones. Some overestimation of both the metal−metal and metal−radical couplings is observed, but there is semiquantitative agreement between the parameters from the fit of the magnetic susceptibility and the calculated ones. The coupling of the NIT-radical with the dicopper moiety is correctly predicted to be antiferromagnetic while the NOA-dicopper exchange interaction is also found to be ferromagnetic in the DFT calculations. Examination of the calculated spin density map shown in Figure 8 for **2** and **3** allows rationalization of the different signs. A major amount of spin density is localized on the two copper(II) centers as well as the ONCNO (**2**) and NO (**3**) moieties. However, the spin density is also spread

(41) Boudalis, A. K.; Raptopoulou, C. P.; Psycharis, V.; Sanakis, Y.; Abarca, B.; Ballesteros, R.; Chadlaoui, M. *Dalton Trans.* **2007**, 3582.
(42) Yoon, J.; Solomon, E. I. *Inorg. Chem.* **2005**, *44*, 8076.

Table 2. Comparison of Experimental and Calculated Exchange Coupling Parameters J and J' for Compounds **1** to **3**

compound	J'_{exp}, cm^{-1}	J_{exp}, cm^{-1}	J'_{calc}, cm^{-1}	J_{calc}, cm^{-1}
Cu−Cu **1**		+28		
NIT−Cu-Cu **2**	−2.3	+28	−7.0	+52.1
NOA−Cu-Cu **3**	+1.5	+28	+6.5	+53.9

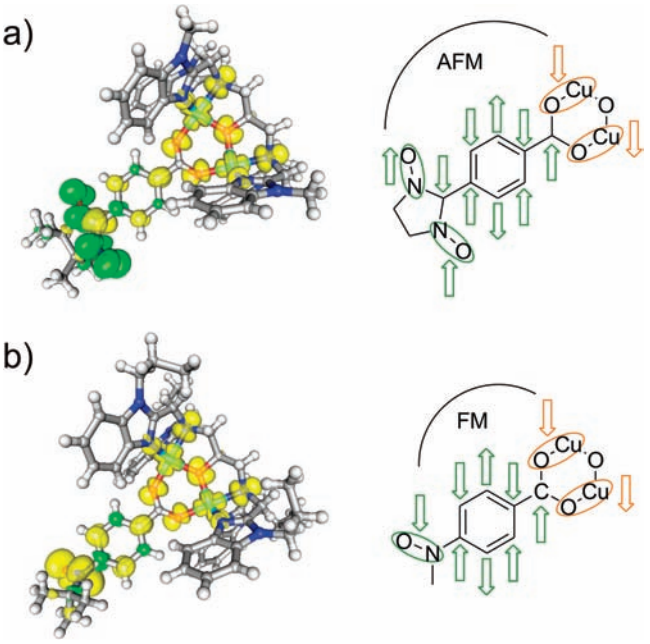

Figure 8. UB3LYP-calculated spin density at an isosurface value of ±0.0015 (left) and schematic representation of the exchange coupling pathway (right) for (a) NIT complex **2** and (b) NOA complex **3**.

out onto the phenyl ring for both the NIT and the NOA case, too. Additional contributions due to direct delocalization are found on the N and O donor atoms directly coordinated to the copper centers.

Previous calculations showed that for the *tert*-butyl nitroxide radical (NOA), a more significant delocalization of spin density onto the phenyl ring takes place compared to the NIT.[43] Theses calculations also revealed the geometric dependence of the spin-delocalization pathway on the tilt angle between the phenyl ring and the spin-bearing moiety. At angles above 20°, which was also found to be the energetically most favored tilt for free NOA, the spin density on the phenyl ring starts to drop significantly because of a loss of conjugation between the NO group and the six-membered ring. On the basis of these calculations, at an angle of 55.7° as found in the crystal structure of **3**, the spin density on the phenyl ring is expected to be only about 20% of the value calculated for near-coplanarity of the NO and phenyl groups. Thus, the large tilt angle is thought to diminish the exchange interaction between the ferromagnetically coupled dicopper unit and the NOA radical. In other systems with smaller angles, an even stronger long-distance metal-radical exchange interaction than the one observed here can be expected.

(43) Schatzschneider, U.; Rentschler, E. *J. Mol. Struct., THEOCHEM* **2003**, *638*, 163.

Conclusion

Stable NIT and *tert*-butyl nitroxide (NOA) radical-functionalized benzoates were coordinated to a dimeric copper(II) unit chelated by a heptadentate benzimidazolate-based N_6O ligand. In a model compound without a paramagnetic substituent on the benzoate, the copper ions are ferromagnetically coupled giving a triplet ground state, as confirmed by magnetic susceptibility measurements and EPR spectroscopy. Investigation of the copper-radical complexes revealed that the Cu−Cu interaction remains essentially unchanged compared to the compound with a diamagnetic bridging ligand because of the almost identical coordination environment of the metal ions in all complexes prepared. Magnetic data and EPR measurements of both copper-radical complexes revealed an additional metal-radical exchange interaction. For the NIT compound, this exchange coupling is antiferromagnetic in nature, whereas the NOA complex shows a ferromagnetic coupling. These results were further confirmed by DFT calculations. The change in sign of the exchange parameter is explained by a shortening of the exchange-coupling pathway by one bond from NIT to NOA. In contrast, previously in similar antiferromagnetically coupled homovalent metal dimers no metal-radical interaction was observable. Thus, by a proper choice of radical ligand and metal unit, it is possible to prepare systems in which the long-distance metal-radical exchange interaction significantly influences the spin ground state of the whole system. It will be of interest to apply this approach also to the preparation of high-spin metal-radical cluster systems. In particular, for NOA systems with small NO-phenyl tilt angles even more significant metal-radical couplings can be expected.

Experimental Section

General Procedures. All chemicals were reagent grade and used as received without further purification. C, H, and N analysis was performed on a Foss Heraeus Vario EL elemental analyzer. Molecular weights and formula are calculated without solvent molecules when not explicitly stated. CW X-band EPR spectra were recorded on a Bruker Elexsys 580 cw/pulse EPR spectrometer, using an ENDOR resonator (MD4EN) ($\nu = 9.772$ GHz). The temperature was varied using a closed cycle cryostat (ARS AF204, customized for CW and pulse EPR, ARS, Macungie, PA, U.S.A.).

All spectral simulations were performed with home-written programs in MATLAB (The MathWorks, Inc.) employing the EasySpin toolbox (v. 3.0.0) for EPR spectroscopy.[44,45] Low-temperature, powder-type EPR spectra were simulated by directly computing the resonance fields and transition probabilities over a triangular orientational powder grid, as implemented in EasySpin.

NMR spectra were recorded using a Bruker DRX 400 spectrometer. Infrared spectra were recorded in the 400 to 4000 cm^{-1} range using a Jasco FT/IR-4200 spectrometer. The IR measurements were carried out using the pellet technique with KBr as embedding medium. For the electrospray ionization mass spectrometry (ESI-MS) a LCQ Finnigan MAT ion trap mass spectrometer was used.

Ligand Synthesis. The ligands HL^{nPr} and NIT−C_6H_4−COOH as well as the sodium salt of the latter were prepared as already reported.[25] The synthesis of NOA−C_6H_4−COOH and its sodium salt NOA−C_6H_4−COONa also followed a

(44) Stoll, S.; Schweiger, A. *J. Magn. Reson.* **2006**, *178*, 42.
(45) Stoll, S.; Schweiger, A. *Biol. Magn. Reson.* **2007**, *27*, 299.

literature procedure.[30] Briefly, NOA−C_6H_4−COOH (5.0 g, 24 mmol) was dissolved in methanol (100 mL). Then, sodium methanolate (1.3 g, 24 mmol) was added, and the mixture stirred until a clear red solution was obtained. The solvent was then removed under reduced pressure to give a red solid which was dried in air, to obtain NOA−C_6H_4−COONa (5.1 g, 92% yield).

Synthesis of Metal Complexes. [$Cu_2(L^{nPr})(O_2N-C_6H_4-COO)](BF_4)_2\cdot CH_3CN$, 1. HL^{nPr} (0.78 g, 1.0 mmol) was dissolved in methanol (40 mL) and then a methanol solution of copper(II)chloride dihydrate (0.34 g, 2.0 mmol) was added while stirring at room temperature. Then, sodium nitrobenzoate (0.28 g, 1.5 mmol) and sodium tetrafluoroborate (0.49 g, 4.5 mmol) were added as a solid, and the resulting suspension stirred at room temperature for 1 h. The blue precipitate formed was filtered off and dried in the air. The crude product was dissolved in acetonitrile and filtered again. Vapor diffusion of diethylether into an acetonitrile solution gave blue crystals of **1** (1.11 g, 82% yield). $C_{54}H_{61}B_2Cu_2F_8N_{11}O_5\cdot H_2O$ (1262.85): calcd. C 51.36, H 5.03, N 12.20; found C 51.05, H 4.97, N 12.13; IR (cm^{-1}): $\tilde{\nu}$ = 3427 (sh) m, 3060 vw, 2988 w, 2935 w, 2877 w, 1573 m, 1496 m, 1452 m, 1406 m, 1347 m, 1295 m, 1080 s, 1034 s, 939 w, 905 w, 747 m, 528 m, 432 vw; ESI-MS: (m/z) = 1156.0 $[M - BF_4]^+$, 535.7 $[M - 2BF_4]^{2+}$.

[$Cu_2(L^{nPr})(NIT-C_6H_4-COO)](ClO_4)_2\cdot 3\ CH_3CN$, 2. HL^{nPr} (0.78 g, 1.0 mmol) was dissolved in methanol (40 mL) and then a methanol solution of copper(copper(II)chloride) perchlorate hexahydrate (0.74 g, 2.0 mmol) was added while stirring at room temperature until a slurry appeared. Then, NIT−C_6H_4−COONa (0.4 g, 1.5 mmol) was added as a solid and the resulting suspension stirred at room temperature for 1 h. The blue precipitate formed was filtered off and dried in the air. The crude product was dissolved in acetonitrile and filtered again. Vapor diffusion of diethylether into an acetonitrile solution gave dark blue-green crystals of **3** (1.17 g, 78% yield). $C_{61}H_{73}Cl_2Cu_2N_{12}O_{13}\cdot 2\ H_2O$ (1416.33): calcd. C 51.73, H 5.48, N 11.87; found C 51.79, H 5.28, N 11.97; IR (cm^{-1}): $\tilde{\nu}$ = 3430 (sh) m, 2987 vw, 2932 w, 2874 w, 1588 m, 1496 m, 1453 m, 1402 m, 1295 m, 1090 s, 904 w, 745 m, 624 m, 528 w, 457 w; ESI-MS: (m/z) = 1280.1 $[M - ClO_4]^+$, 590.7 $[M - 2ClO_4]^{2+}$.

[$Cu_2(L^{nPr})(NOA-C_6H_4-COO)](PF_6)_2\cdot 0.5\ MeOH\cdot 2\ H_2O$, 3. HLnPr (0.78 g, 1.0 mmol) was dissolved in methanol (40 mL) and then a methanol solution of copper(II)chloride dihydrate (0.34 g, 2.0 mmol) was added while stirring at room temperature. Then, NOA−C_6H_4−COONa (0.35 g, 1.5 mmol) was added as a solid and the resulting suspension stirred at room temperature for 1 h. The red precipitate formed was filtered off and dried in the air. The crude product was dissolved in acetonitrile and filtered again. Vapor diffusion of diethylether into an acetonitrile solution gave orange crystals of 3 (0.97 g, 69% yield). $C_{58}H_{70}Cu_2F_{12}N_{11}O_4P_2\ \cdot H_2O$ (1420.28): calcd. C 49.05, H 5.11, N 10.85; found C 49.22, H 4.53, N 10.95; IR (cm^{-1}): $\tilde{\nu}$ = 3458 (sh) m, 3080 vw, 2988 w, 2935 w, 2877 w, 1589 m, 1544 m, 1486 m, 1453 m, 1407 m, 1361 m, 1293 m, 1255 m, 1092 s, 982 w, 939 w, 898 w, 748 m, 622 m, 507 vw, 437 vw; ESI-MS: (m/z) = 1238.9 $[M - PF_6 - O]^+$, 1224.0 $[M - PF_6 - O - CH_3]^+$.

Computational Details. All calculations were carried out as single point runs using the coordinates available from the X-ray structure determinations with ORCA 2.6.35 on a Dell Optiplex 745 computer running Ubuntu 4.2.3 as the operating system.[46] Counterions and solvate molecules were removed to only treat the cationic unit. Alkyl substituents on the benzimidazolyl groups were truncated to methyl, with the hydrogen atom placed along the original C−C axis at an average distance. The unrestricted B3LYP functional was used in the calculation of the spin-density distribution and energies, with a TZVP basis set on the metal and radical centers as well as the donor atoms directly coordinated to the metal.[47] For all other atoms, a DZ(P) basis was employed.[48] Because of the very small energy differences expected, a very tight convergence criterion (option *VeryTightSCF*, energy change TolE < 10^{-8} Eh) together with a Lebedev-434 grid (option *Grid5*) was used. Starting from the converged high spin state, the other relevant states could easily be obtained with the *FlipSpin* option. The orbital occupation and spin density distribution was inspected in each case to verify convergence to the desired open-shell state.

X-ray Crystallographic Data Collection and Refinement of the Structures. Single crystals of **1** to **3** were coated with perfluoropolyether, picked up with a glass fiber, and mounted on a SMART APEX II CCD diffractometer equipped with a nitrogen cold stream operating at 171(2) K. Graphite monochromated Mo Kα radiation (λ = 0.71069 Å) from a fine-focus sealed tube was used throughout. The crystallographic data of the compounds are listed in Table 1. Cell constants were obtained from a least-squares fit of the diffraction angles of several thousand strong reflections. The data reduction was done with APEX2 v2.0,[49] while for the structure solution SIR-97[50] and for the refinement SHELXL-97[51] were used. No absorption correction was employed. Crystallographic data (excluding structure factors) for the structures reported in this paper have been deposited with the Cambridge Crystallographic Data Center as supplementary publications nos. CCDC-699686, -699605, and -699685, for structures **1**, **2**, and **3** respectively. Copies of the data can be obtained free of charge on application to CCDC, 12 Union Road, Cambridge, CB2 1EZ, UK [Fax: (internat.) 14421223/3362033; E-mail: deposit@ccdc.cam.ac.uk].

Acknowledgment. U.S. thanks Prof. Dr. Nils Metzler-Nolte (Bochum) for generous access to the computational infrastructure of the institute. E.R. thanks Christopher Reinnig and Lars Müller (Mainz) for recording the ESI mass spectra.

(46) Neese, F.; *ORCA*, version 2.6.35.
(47) Schafer, A.; Horn, H.; Ahlrichs, R. *J. Chem. Phys.* **1992**, *97*, 2571.
(48) The Ahlrichs DZ basis set was obtained from the TurboMole basis set library under ftp.chemie.uni-karlsruhe.de/pub/basen.
(49) *Bruker 2005 APEX2 Software Suite version* 2.0.
(50) Altomare, A.; Burla, M. C.; Camalli, M.; Cascarano, G. L.; Giacovazzo, C.; Guagliardi, A.; Moliterni, A. G. G.; Polidori, G.; Spagna, R. *J. Appl. Crystallogr.* **1999**, *32*, 115.
(51) Sheldrick, G. M. *SHELXL-97, Program for Crystal Structure Refinement*; University of Göttingen: Göttingen, Germany.